Published in final edited form as:
Bone. 2005 September ; 37(3): 379–387. doi:10.1016/j.bone.2005.04.004.

Mapping bone interstitial fluid movement: Displacement of ferritin tracer during histological processing

Cesare Ciani[a], **Stephen B. Doty**[b], and **Susannah P. Fritton**[a,*]

[a]Department of Biomedical Engineering, City College of New York/CUNY, Convent Avenue at 138th Street, New York, NY 10031, USA

[b]Research Division, Hospital for Special Surgery, New York, NY 10021, USA

Abstract

Bone interstitial fluid flow is thought to play a fundamental role in the mechanical stimulation of bone cells, either via shear stresses or cytoskeletal deformations. Recent evidence indicates that osteocytes are surrounded by a fiber matrix that may be involved in the mechanotransduction of external stimuli as well as in nutrient exchange. In our previous tracer studies designed to map how different-sized molecules travel through the bone porosities, we found that injected ferritin was confined to blood vessels and did not pass into the mineralized matrix. However, other investigators have shown that ferritin forms halo-shaped labeling that enters the mineralized matrix around blood vessels. This labeling is widely used to explain normal interstitial fluid movement in bone; in particular, it is said to demonstrate bulk centrifugal interstitial fluid movement away from a highly pressurized vascular porosity. In addition, appositional ferritin fronts are said to demonstrate centrifugal interstitial fluid movement from the medullary canal to the periosteal surface. The purpose of this study was to investigate the conflicting ferritin labeling results by evaluating the role of different histological processes in the formation of ferritin "halos." Ferritin was injected into the rat vasculature and allowed to circulate for 5 min. Samples obtained from tibiae were reacted for different times with Perl's reagent and then were either paraffin-embedded or sectioned with a cryostat. Halo-like labeling surrounding vascular pores was found in all groups, ranging from 1.2–3.9% for the samples treated with the shortest histological processes (unembedded, frozen sections) to 5.6–15% for the samples treated with the longest histological processes (paraffin-embedded sections). These results indicate that different histological processing methods are able to create ferritin "halos," with some processing methods allowing more redistribution of the ferritin tracer than others. Based on these results and the fact that "halo" labeling has not been found with any other tracer, as we seek to further delineate the movement of interstitial fluid and the role it plays in bone mechanotransduction, we believe that ferritin "halo" labeling should not be used to demonstrate physiological bone interstitial fluid flow.

Keywords

Bone permeability; Physiological transport; Bone metabolism; Osteocyte; Lacunar–canalicular porosity

*Corresponding author. Fax: +1 212 650 6727. fritton@ccny.cuny.edu (S.P. Fritton)..

Introduction

Interstitial fluid flow is thought to play an important role in bone's mechanosensory system by activating bone cells via shear stresses [9,12,25] or cytoskeletal deformations [27]. Bone interstitial fluid flow is also believed to aid in delivering nutrients and transporting metabolic waste products from the bone cells [17]. To better understand interstitial fluid movement in bone, techniques using markers or tracers such as procion red (300–400 Da, diameter <1 nm), reactive red (1470 Da, diameter ~1 nm), microperoxidase (1860 Da, diameter ~2 nm), horseradish peroxidase (40 kDa, diameter ~6 nm), ferritin (440 kDa, diameter ~12 nm [20]), and different-sized dextrans (range 300 Da–2000 kDa, diameter ~1 nm–60 nm) have been used to map how different sized molecules travel through the various porosities in bone [1,5,8,13–16,19,22–24].

The architecture of cortical bone has three levels of porosity: the vascular porosity, the lacunar–canalicular porosity, and the collagen–apatite porosity of the mineralized matrix. The vascular porosity of animals without a secondary osteonal structure, such as rats and mice, consists of primary canals and transverse canals; this porosity is the largest of the three bone porosities (order 20 μm, [2]). The lacunar–canalicular porosity is formed by the space surrounding the osteocytes in the lacunae and canaliculi (order 100 nm, [28]). Within the canaliculi, a pericellular fiber matrix is believed to keep the osteocyte processes in position, connecting them to the canalicular wall [25,27] and preventing them from collapsing [28]. The fiber matrix spacing is believed to be approximately 7–8 nm, similar to the surface glycocalyx on endothelial cells, and the fiber matrix has been proposed to work as a sieve, allowing only molecules smaller than the pore diameter to pass through [3,21,25]. Lastly, the smallest bone porosity is the collagen–apatite porosity associated with the space between the collagen fibers and the crystallites of mineral apatite. The dimensions of this porosity have not been well characterized, and there is contradictory evidence from tracer studies as to whether molecules <10 nm can pass into the mineralized matrix [22,24].

Our previous tracer studies indicate that ferritin injected into rats is confined to the bone blood vessels and does not pass into the mineralized matrix [24]. However, other investigators have shown that ferritin forms halo-shaped labeling that appears to enter the mineralized matrix around blood vessels, along with appositional fronts along the bone surfaces [5,15,16,19]. This ferritin labeling is widely used to explain normal interstitial fluid movement in bone: the halos are said to demonstrate bulk centrifugal interstitial fluid movement away from a highly pressurized vascular porosity, and the appositional fronts are said to demonstrate centrifugal interstitial fluid movement from the medullary canal to the periosteal surface [5,6,9–11,15,16,19,26]. These previous studies suggest that ferritin may be small enough to pass through the canalicular pores and possibly through the collagen–apatite pores in the mineralized matrix.

The contradictory ferritin findings and the fact that ferritin is the only tracer that has demonstrated “halo” labeling around blood vessels pushed us to investigate in further detail the movement of ferritin in the bone porosities. Based on our previous work with ferritin, our hypothesis was that the halo-shaped ferritin labeling found by other investigators was the result of histological processing methods. In this study, we evaluated the role of different histological processing steps in the formation of ferritin “halos.”

Methods

In vivo injection of Type I horse spleen ferritin (440 kDa, diameter ~12 nm, Sigma, St. Louis, MO) was performed on male Sprague–Dawley rats (n = 5, 320–340 g, 10–11 weeks

old). An additional animal (n = 1, 280 g, 9 weeks old) was injected with saline buffer solution as control.

Permission for this in vivo study was granted by the Institutional Animal Care and Use Committee at the Hospital for Special Surgery. Rats were first anesthetized via an intraperitoneal injection of a mixture of ketamine (80 mg/kg body weight) and xylazine (5 mg/kg body weight). The left jugular vein was then exposed surgically and a 25G5/8 needle attached to a 3-ml syringe was inserted into the vein to inject a bolus of tracer solution. Our previous experiments showed that ferritin was best detected if injected at a dosage of at least 150 mg/100 g of body weight [24]. We concentrated the ferritin solution using Amicon Ultra-4 centrifugal filter devices (100,000 molecular weight cutoff, Millipore, Billerica, MA), from 85 mg/ ml to a final solution of 309 mg/ml. The final concentrated ferritin solution was delivered at 190 mg/100 g of body weight with a total volume of 2 ml. After the tracer was injected (injection time 2 min), it was allowed to freely circulate for 5 min. The rats were then sacrificed with carbon dioxide inhalation and both tibiae and femora were harvested. Femora were put immediately in Karnovsky's fixative (3% glutaraldehyde, 3% paraformaldehyde in 0.2 M sodium potassium phosphate), while tibiae were cut at the mid-diaphyses into two parts and then placed in Karnovsky's fixative.

From each injected animal, one 6-mm block was cut from the right tibia, while from the left tibia, five 2-mm blocks were cut using a diamond blade saw (Buehler, Lake Bluff, IL) (Fig. 1). All the samples were placed in Perl's reagent (1:1 solution of 2% HCl and 2% potassium ferro-cyanide), which allowed potassium ferrocyanide to combine with the ferric ion to form the characteristic end product Prussian Blue that enables visualization of the ferritin under light microscopy.

Histological processing of bone groups

The goal of this study was to determine if different histological processing methods affect the production of ferritin “halos.” Six different histological processes were performed to determine if a particular processing method would be able to transport ferritin into the mineralized matrix (Table 1). These processing methods were similar to or variations of the methods used in our previous ferritin study [24] as well as previous studies where the movement of ferritin into the mineralized matrix produced a characteristic “halo” of blue stain around the blood vessels [5,16]. The six blocks taken from each animal were divided into two groups and each group was labeled according to its major histological process: the first group (two blocks) was designated PARA (for paraffin embedding), while the second group (4 blocks) was designated FROZ (for frozen section, no embedding).

Paraffin-embedded samples (blocks PARA3, PARA8)—After 48 h in Karnovsky's fixative, the samples PARA3 and PARA8 were put in Perl's reagent for 3 or 8 h, respectively. They were then decalcified in 10% nitric acid for 5 days (samples PARA3) or in citrate formic acid [18] for 8 days (samples PARA8) [5,16]. Samples were placed in a series of graded alcohol (50%, 70%, 95%, and 100%), then xylene, and then were embedded in paraffin. Thin sections (5–7 Am thick) were cut using a microtome (Reichert-Jung 2030, Germany), dried overnight in an oven, deparaffinized, counterstained with hematoxylin to achieve a pink background, and coverslipped with mounting media (Richard-Allan Scientific, Kalamazoo, MI).

Frozen, unembedded samples (blocks FROZ1, FROZ3, FROZ8, FROZ24)—After 48 h in Karnovsky's fixative, the samples were put in Perl's reagent for 1 h (samples FROZ1), 3 h (samples FROZ3), 8 h (samples FROZ8), or 24 h (samples FROZ24).

The blocks FROZ1 and FROZ3 were decalcified in 10% nitric acid for 24 h while FROZ8 and FROZ24 samples could be immediately cut without being further decalcified. The blocks were embedded in OCT medium (Tissue Tek) to provide support during cryosectioning. Thin cross sections (10–15 μm thick) were cut from the blocks using a cryostat (Model OTF 5030, Bright Instrument Company, England). The sections were then counterstained using 0.1% acid fuchsin for 15 s to achieve a pink background, rinsed briefly in distilled water, and coverslipped with aqueous mounting media (Biomeda Corp., Foster City, CA).

To determine mineral content in the samples, the von Kossa treatment was performed on femur specimens. Twomm-thick specimens were cut from the femur mid-diaphysis using the diamond blade saw and put in Karnovsky's fixative for 24 h. They were then placed in Perl's reagent for 1, 3, 5, 8, or 24 h and embedded in PMMA. Thin cross sections (5–10 μm) were cut from each block and analyzed under light microscopy to qualitatively measure the mineralized area of the section. The mineral distribution is visualized by the brown/black color resulting from the reaction of the mineral present in the section and the silver nitrate in the von Kossa solution. A high degree of mineralization results in very black sections, while demineralized sections do not present the characteristic black color. Sections partially mineralized show a varying degree of black according to the mineral content.

To further investigate the Perl's action, we placed a 3-mm block from the control animal injected with saline solution into freshly made Perl's solution for 3 h. In addition, a 3-mm block from the control animal was placed in Perl's reagent in which a sample from a ferritin-injected animal had previously been placed and reacted for 8 h. This control sample was left in the previously used Perl's solution for 24 h.

Microscopic imaging and data analysis

To analyze the tracer distribution in the bone, one cross section was chosen from each animal for each treatment. Sections with a complete cross-sectional area and little cutting damage were chosen for analysis. The sections were analyzed under routine light microscopy (Nikon Microphot-FXA, Japan). For each section, we counted the total number of blood vessels (N.Bv), the number of blood vessels labeled with ferritin (N.Bv.La), the number of osteocytes labeled with ferritin (N.Ot.La), and the number of “halos” surrounding blood vessels (N.Ha). The data were collected using the BIOQUANT image analysis system (BIOQUANT Image Analysis Corp., Nashville, TN), and images of each halo were recorded. The means and standard deviations of the measurements were calculated for each histological process. When counting the blood vessels, no distinction was made between blood vessels cut longitudinally or in cross section. Halos were identified as both total or partial well-defined ferritin lines around blood vessels (Figs. 2a, e) as well as more spread-out diffusive movement of ferritin in the extravascular region (Fig. 2d). For all the samples, the blood vessels were counted using the 10× objective, while the halos and the osteocytes labeled with ferritin were counted with the 20× objective.

The percentage of labeled blood vessels (i.e., labeled blood vessels/total number of blood vessels, N.Bv.La/ N.Bv), the percentage of labeled osteocytes (N.Ot.La/ N.Ot), and the percentage of blood vessels surrounded by halos (N.Ha/N.Bv) were calculated and analyzed using oneway ANOVA. One-way ANOVA was used because we only wanted to determine if the different processing methods could influence the percentage of blood vessels surrounded by ferritin halos; the study was not designed to determine which component of the processing methods is responsible for producing halo labeling. Statistical analysis was performed to determine differences between the histological processes using SPSS for Windows version 12.0 (SPSS Inc., Chicago, IL). For all the statistical tests, a significance level of $P < 0.05$ was used.

Results

Ferritin, localized by the Perl's reaction, was effectively delivered to the blood vessels for all treatments (Figs. 2a through e). However, while the ferritin was able to reach most of the bone blood vessels, there was no ferritin labeling surrounding the osteocytes. The percentage of blood vessels labeled with ferritin ranged from 79% to 95%, while the percentage of labeled osteocytes was 0% for all the treatments (Table 2, Fig. 3). The percentage of labeled blood vessels for both paraffin groups was lower than the unembedded, frozen-sectioned groups.

Measurements at a magnification of 20× showed ferritin “halos” in all sections of each group. The percentage of blood vessels surrounded by halos ranged from 1.2 to 15% (Table 2, Fig. 4). The frozen-sectioned groups showed a similar percentage of blood vessels surrounded by halos (1.2–3.9%), while the paraffin-embedded PARA8 group was significantly larger than all other groups (15%), and the PARA3 group was significantly different from FROZ24 (Fig. 4).

In all the sections, the endosteal surface was well defined by a blue line along the perimeter, and a ferritin appositional front was also visible (Figs. 2b, e); the edge of the periosteal surface was also stained (Fig. 2c). Sections from the control animal that did not receive injection of ferritin did not show any characteristic blue staining occurring from the reaction of Perl's and ferritin. However, sections from the control animal that were placed in Perl's solution previously used with a sample from a ferritin-injected animal showed a marked periosteal blue line and also the presence of halos around blood vessels (Fig. 2f).

The von Kossa method indicated that the percent mineralized area of the specimens decreased proportionally to the time placed in Perl's reagent (Fig. 5). Samples that stayed in Perl's reagent for 1 h showed very little demineralization. Samples that stayed longer than 5 h in the reagent were almost completely decalcified. A total degree of decalcification was achieved by samples that stayed for 24 h in the reagent.

Discussion

We were able to produce ferritin “halo” labeling with all the different histological treatments used. The percentage of blood vessels surrounded by halos was quite low, ranging from 1.2–3.9% for the samples treated with the shortest histological processes (unembedded, frozen sections) to 5.6–15% for the samples treated with the longest histological processes (paraffin-embedded sections). Our measurements, taken at a magnification of 20×, are similar to those reported by other investigators (7.6% at 10×, 26% at 40×) [15].

The only significant differences between groups were found between the paraffin-embedded samples and the unembedded, frozen-sectioned samples. The groups PARA3 and PARA8 had the lowest percentage of blood vessels labeled with ferritin (Fig. 3), and PARA8 had the highest percentage of blood vessels surrounded by halos (Fig. 4). The differences may be explained by the differences in the embedded vs. unembedded histological processes. The frozen blocks were fixed, reacted with Perl's reagent, decal-cified (groups FROZ3 and FROZ8 only), and sectioned within 3 days after the injection with a minimum loss of tracer. The paraffin-embedded samples were fixed, reacted with Perl's reagent, completely decalcified, washed, dehydrated in ascending grades of alcohol, cleared in xylene, embedded in paraffin, sectioned, cured in an oven, deparaffinized, and counterstained. This process took approximately 9 days, in which samples were kept in solutions that greatly differ from the in vivo environment where they live and interact with physiological fluid. Such a long processing time in so many solutions might also facilitate the movement of ferritin, resulting both in a reduction of blood vessels labeled with ferritin along with the formation of “halos.”

The finding of ferritin halos in the FROZ1 samples, which were treated similarly to the methods we used in our previous study that showed ferritin completely confined to the vascular pores with no “halos” [24], is probably due to the area we chose to count the blood vessels. In the present study, we analyzed the ferritin distribution over the entire bone sectional area, while in our previous study, we only considered the tracer distribution in three distinct sectors of the tibia: anterior, lateral, and medial. By only considering three subareas of the cross section, we likely overlooked the ~4% halo labeling found for the FROZ1 sections in the present study. Another difference between the present study and our previous study that could possibly affect the results was that Karnovsky's fixative was used instead of alcohol to better mimic processing by previous investigators [5,15,16,19].

While this study was only designed to test whether histological processing techniques used by other investigators could produce ferritin “halo” labeling (it was not designed to determine which portion of the histological processing produces ferritin “halos”), a possible explanation for the production of halo-like ferritin labeling is that some component of the histological processing creates structural changes in the bone matrix. Ferritin is a spherical molecule, composed of a protein-assembled shell and an iron core. In order to visualize ferritin, samples are placed in Perl's reagent, which dissolves ferritin's protein shell and reacts with the iron core to produce the characteristic Prussian blue utilized to visualize this tracer under light microscopy [4,7]. Perl's reagent is able to dissolve the protein core because it is a very strong acid (pH 0.89). To evaluate the effect of the Perl's reagent on the bone mineral, we analyzed the specimens treated with von Kossa, and it was possible to see a clear trend of bone decalcification caused by the interaction between the Perl's reagent and bone tissue (Fig. 5). Thus, the acidic activity of the reagent might influence the sieving structure of the bone: as the acidic reagent removes bone crystallites from the mineralized matrix, injected unbound ferritin may be able to penetrate the increasingly porous bone, thus creating “halos.” However, it should be noted that there was no clear trend between the length of time bone samples were placed in Perl's reagent and the percentage of blood vessels surrounded by “halos.”

Another peculiarity of ferritin reacting with Perl's reagent is that, during the reaction, ferritin molecules are disassembled and then recombined, giving rise to a final molecule with a smaller diameter than the original one [7]. This reduction in diameter might also facilitate the propagation and diffusion of ferritin outside the vascular canal into the dissolving mineralized matrix. Moreover, the presence of halos and a ferritin appositional front found in control samples from an animal that did not receive injected ferritin but was placed in already used Perl's reagent strongly indicates the possibility of histological artifact caused by the Perl's reagent (Fig. 2f). In this case, since no ferritin was injected in vivo into the animal circulation, the halo labeling could be attributed to the demineralizing action of the Perl's solution acting on the sections, and the consequent movement of ferritin present in the solution into the bone matrix. No ferritin labeling was found in control samples placed in fresh Perl's solution.

While the idea of tracking a molecule inside bone tissue is very simple, bone is a very dense yet delicate tissue, and histological processes, if not well designed, can lead to a wrong interpretation of the real bone physiology. Due to the high tissue mineral content, bone histology can be a very long and complicated process. Bone samples have to pass through many different steps before being sectioned and analyzed under the microscope. Each solution where the samples stay (i.e., acidic solutions for decalcification, dehydrating solutions, embedding media) could cause loss of biological information and, at the same time, generate unreliable results. The demineralization process might provoke an unexpected enlargement of the original pore dimensions, allowing the passage of larger molecules, such as ferritin, otherwise prohibited. Moreover, the visualization of ferritin requires a critical

step, the reaction with Perl's reagent, which reacts with the iron moiety of ferritin to form Prussian blue, never accounted for as a possible source of artifact.

Previous tracer studies using ferritin have explained ferritin “halos” as being generated by a centrifugal fluid force acting in the intravascular domain, driving the ferritin outside the vascular wall and into the mineralized matrix. In addition, appositional fronts along the bone surfaces have been said to demonstrate centrifugal interstitial fluid movement from the medullary canal to the periosteal surface [5,6,9–11,15,16,19,26]. The purpose of this study was to analyze the effect of different histological processes that could lead to the presence of ferritin in the mineralized matrix and the characteristic ferritin halo labeling previously demonstrated by other investigators. We were able to demonstrate that while all processing methods produced ferritin “halos,” the paraffin embedding procedure produced a higher percentage of blood vessels surrounded by halos compared to the other groups. Based on these results and the fact that “halo” labeling has not been found with any other tracer, as we seek to further delineate the movement of interstitial fluid and the role it plays in bone mechanotransduction, we believe that ferritin “halo” labeling should not be used to demonstrate physiological bone interstitial fluid flow. The use of additional tracers of dimensions comparable to ferritin will help to better understand the porosity sizes governing interstitial fluid movement in bone.

Acknowledgments

The authors would like to thank Orla O’Shea, Janane N. Diouri, Anthony Labissiere, and Dr. Francesca Orlandi for their technical support. This study was supported by research grants from the NIH (NIAMS, AR46429) and the Whitaker Foundation (RG-01-0440).

References

1. Ayasaka N, Kondo T, Goto T, Kido MA, Nagata E, Tanaka T. Differences in the transport systems between cementocytes and osteocytes in rats using microperoxidase as a tracer. Arch Oral Biol. 1992; 37:363–9. [PubMed: 1610305]
2. Cooper RR, Milgram JW, Robinson RA. Morphology of the osteon. An electron microscopy study. J Bone Joint Surg. 1966; 48A:1239–71. [PubMed: 5921783]
3. Cowin SC, Weinbaum S, Zeng Y. A case for bone canaliculi as the anatomical site of strain generated potentials. J Biomech. 1995; 28:1281–97. [PubMed: 8522542]
4. Cowley JM, Janney DE, Gerkin RC, Buseck PR. The structure of ferritin cores determined by electron nanodiffraction. J Struct Biol. 2000; 131:210–6. [PubMed: 11052893]
5. Dillaman RM. Movement of ferritin in the 2-day-old chick femur. Anat Rec. 1984; 209:445–53. [PubMed: 6476415]
6. Dillaman RM, Roer RD, Gay DM. Fluid movement in bone: theoretical and empirical. J Biomech. 1991; 24:163–77. [PubMed: 1791176]
7. Domínguez-Vera JM, Colacio E. Nanoparticles of prussian blue ferritin: a new route for obtaining nanomaterials. Inorg Chem. 2003; 42:6983–5. [PubMed: 14577762]
8. Doty, SB.; Schofield, BH. Metabolic and structural changes within osteocytes of rat bone.. In: Talmage, RV.; Munson, PL., editors. Calcium, parathyroid hormone and the calcitonins. Elsevier; Amsterdam: 1972. p. 353-64.
9. Hillsley MV, Frangos JA. Bone tissue engineering: the role of interstitial fluid flow. Biotechnol Bioeng. 1994; 43:573–81. [PubMed: 11540959]
10. Keanini RG, Roer RD, Dillaman RM. A theoretical model of circulatory interstitial fluid flow and species transport within porous cortical bone. J Biomech. 1995; 28:901–14. [PubMed: 7673258]
11. Kelly PJ, Montgomery RJ, Bronk JT. Reaction of the circuatory system to injury and regeneration. Clin Orthop. 1990; 254:275–288. [PubMed: 2182256]

12. Klein-Nulend J, van der Plas A, Semeins CM, Ajubi NE, Frangos JA, Nijweide PJ, Burger EH. Sensitivity of osteocytes to biomechanical stress in vitro. FASEB J. 1995; 9:441–5. [PubMed: 7896017]

13. Knothe Tate ML, Niederer P, Knothe U. In vivo tracer transport through the lacunocanalicular system of rat bone in an environment devoid of mechanical loading. Bone. 1998; 22:107–17. [PubMed: 9477233]

14. Knothe Tate ML, Steck R, Forwood MR, Niederer P. In vivo demonstration of load-induced fluid flow in the rat tibia and its potential implications for processes associated with functional adaptation. J Exp Biol. 2000; 203:2737–45. [PubMed: 10952874]

15. Mak AF, Qin L, Hung LK, Cheng CW, Tin CF. A histomorphometric observation of flows in cortical bone under dynamic loading. Micro-vasc Res. 2000; 59:290–300.

16. Montgomery RJ, Sutker BD, Bronk JT, Smith SR, Kelly PJ. Interstitial fluid flow in cortical bone. Microvasc Res. 1988; 35:295–307. [PubMed: 3393091]

17. Piekarski K, Munro M. Transport mechanism operating between blood supply and osteocytes in long bones. Nature. 1977; 269:80–2. [PubMed: 895891]

18. Presnell, JK.; Schreibman, MP.; Humason, GL. Humason's animal tissue techniques. 5th ed.. Johns Hopkins Univ. Press; 1997.

19. Qin L, Mak AT, Cheng CW, Hung LK, Chan KM. Histomorphological study on pattern of fluid movement in cortical bone in goats. Anat Rec. 1999; 255:380–7. [PubMed: 10409810]

20. Quintana C, Cowley JM, Marhic C. Electron nanodiffraction and high-resolution electron microscopy studies of the structure and composition of physiological and pathological ferritin. J Struct Biol. 2004; 147:166–78. [PubMed: 15193645]

21. Squire JM, Chew M, Nneji G, Neals C, Barry J, Michel C. Quasi-periodic substructure in the microvessel endothelial glycocalyx: a possible explanation for molecular filtering? J Struct Biol. 2001; 136:239–255. [PubMed: 12051903]

22. Tami AE, Schaffler MB, Knothe Tate ML. Probing the tissue to subcellular level structure underlying bone's molecular sieving function. Biorheology. 2003; 40:577–90. [PubMed: 14610309]

23. Tanaka T, Sakano A. Differences in permeability of microperoxidase and horseradish peroxidase into the alveolar bone of developing rats. J Dent Res. 1985; 64:870–6. [PubMed: 3858312]

24. Wang L, Ciani C, Doty SB, Fritton SP. Delineating bone's interstitial fluid flow pathway in vivo. Bone. 2004; 34:499–509. [PubMed: 15003797]

25. Weinbaum S, Cowin SC, Zeng Y. A model for the excitation of osteocytes by mechanical loading-induced bone fluid shear stresses. J Biomech. 1994; 27:339–60. [PubMed: 8051194]

26. Winet H. A bone fluid flow hypothesis for muscle pump-driven capillary filtration: II. Proposed role for exercise in erodible scaffold implant incorporation. Eur Cell Mater. 2003; 6:1–11. [PubMed: 14562269]

27. You L, Cowin SC, Schaffler MB, Weinbaum S. A model for strain amplification in the actin cytoskeleton of osteocytes due to fluid drag on pericellular matrix. J Biomech. 2001; 34:1375–86. [PubMed: 11672712]

28. You LD, Weinbaum S, Cowin SC, Schaffler MB. Ultrastructure of the osteocyte process and its pericellular matrix. Anat Rec. 2004; 278A:505–13.

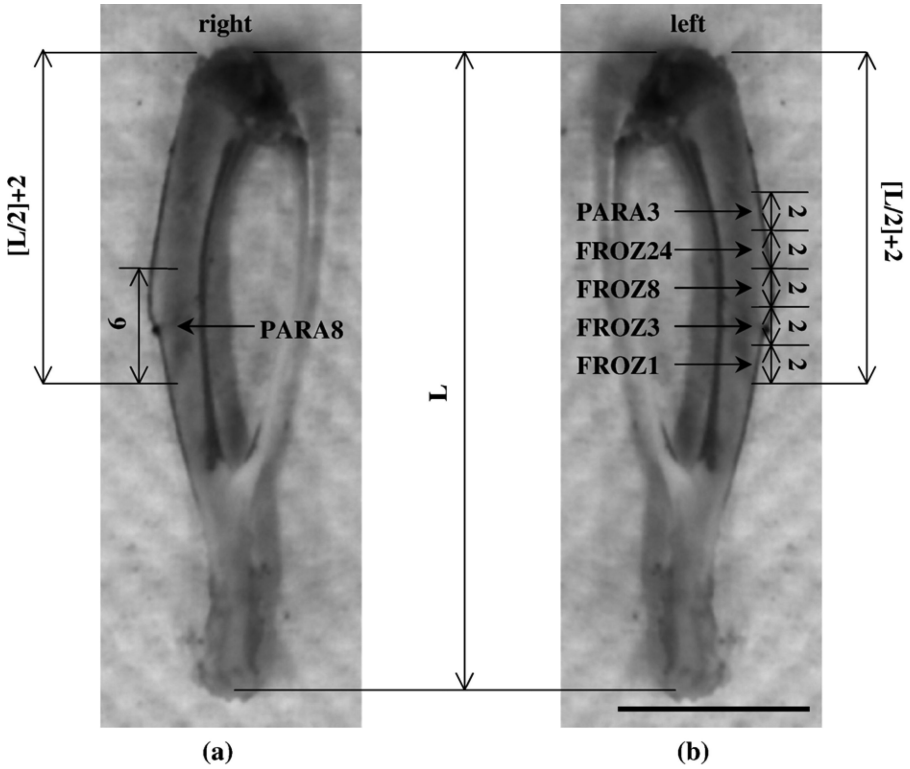

Fig. 1.

Rat right tibia (a) and left tibia (b) showing the locations where the samples were taken for the six different histological processes. The samples were named according to the histological process along with the time they were left in Perl's reagent. FROZ1, 3, 8, 24: frozen, unembedded samples left in Perl's reagent for 1, 3, 8, or 24 h, respectively; PARA3, 8: paraffin-embedded samples left in Perl's reagent for 3 or 8 h, respectively. L = tibia length. All dimensions are in millimeters (scale bar: 10 mm).

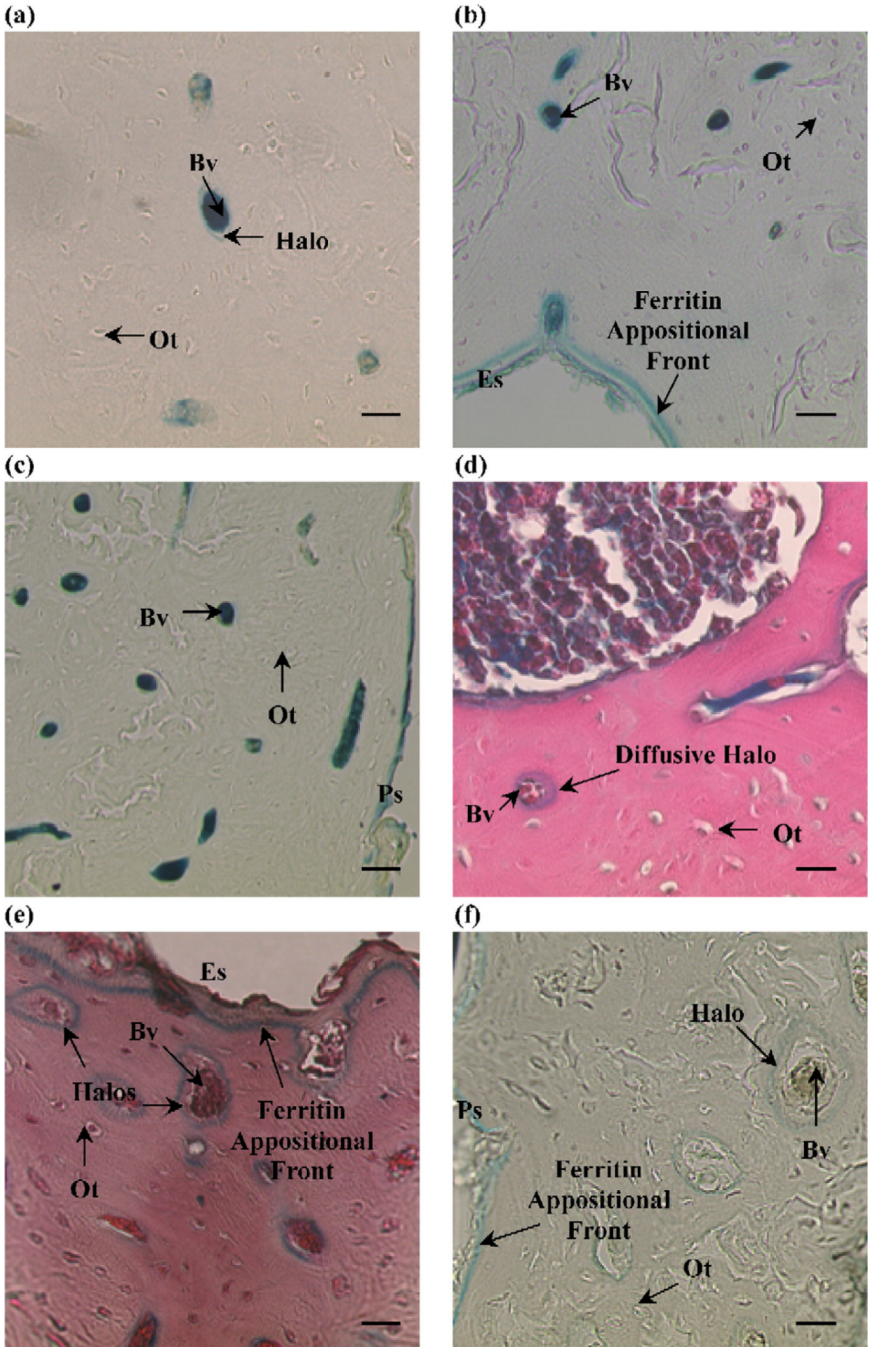

Fig. 2.

Ferritin distribution for the different histological processes; no osteocytes (Ot) were labeled with ferritin for all the processes. (a) Group FROZ1: ferritin was primarily confined to the bone blood vessels (Bv) with the sporadic presence of ferritin “halos”surrounding blood vessels (magnification: 900×, scale bar: 15 μm). (b) Group FROZ3: a ferritin appositional front at the endosteal surface (Es) was clearly visible for all the histological treatments (magnification:450× , scale bar: 30 μm). Group FROZ8 (not pictured) was very similar to FROZ3. (c) Group FROZ24: this group presented the lowest percentage of blood vessels surrounded by halos (magnification: 450×, scale bar: 30 μm). The periosteal surface (Ps) was also labeled with ferritin in all groups. (d) Group PARA3: diffusive halos were seen as

more spread-out or diffusive movement of ferritin in the mineralized matrix surrounding blood vessels (magnification: 900×, scale bar: 15 μm). (e) Group PARA8: this group had the highest percentage of blood vessels surrounded by halos; a strong ferritin appositional front can also be seen at the endosteal surface of the bone (magnification: 900×, scale bar: 15 μm). (f) Halos surrounding blood vessels were also found in the control specimen after it was placed in already used Perl's solution for 24 h; a ferritin appositional front is visible at the periosteal surface (Ps) (magnification: 10×, scale bar: 30 μm).

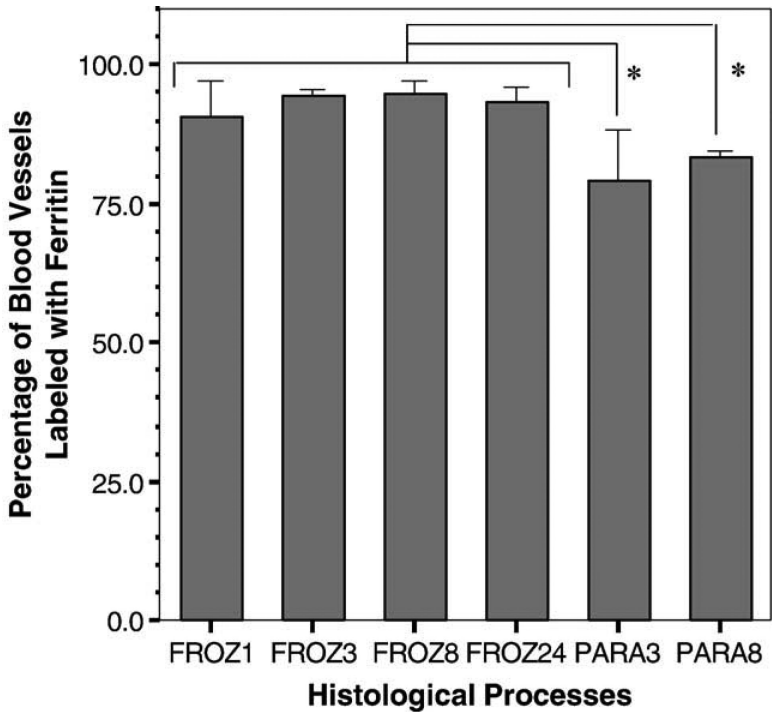

Fig. 3.

Percentage of blood vessels labeled with ferritin for the six histological processing methods (values are reported as mean ± standard deviation). The groups processed using unembedded frozen sections (FROZ) show a higher percentage of labeled blood vessels compared to paraffin-embedded (PARA) groups. The asterisks indicate statistically significant differences between the two PARA groups and all the FROZ groups (*$P < 0.05$).

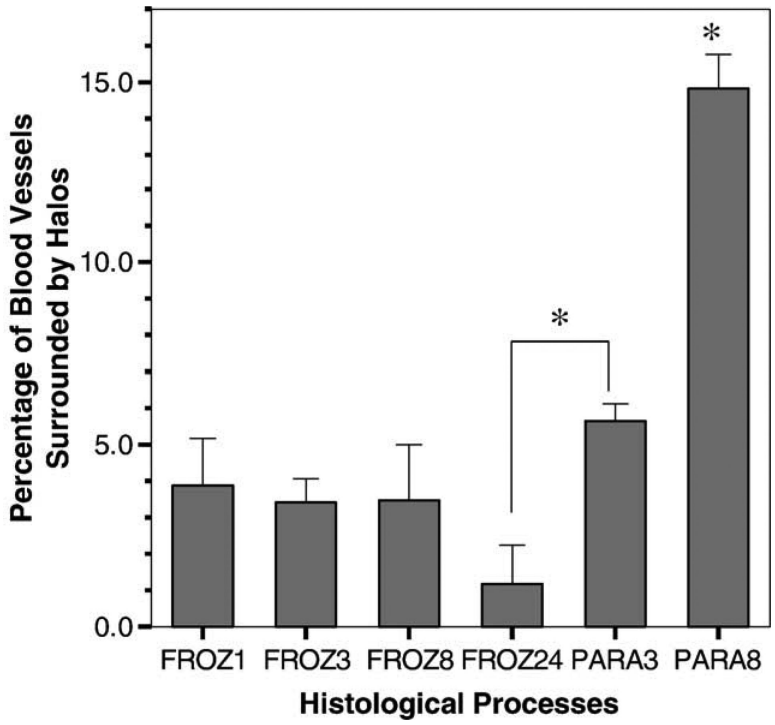

Fig. 4.

The percentage of blood vessels surrounded by halos for the six histological processing methods (values are reported as mean ± standard deviation). The paraffin-embedded group PARA8 was significantly different from all the other groups, while the paraffin-embedded PARA3 was significantly different from FROZ24 (*$P < 0.05$).

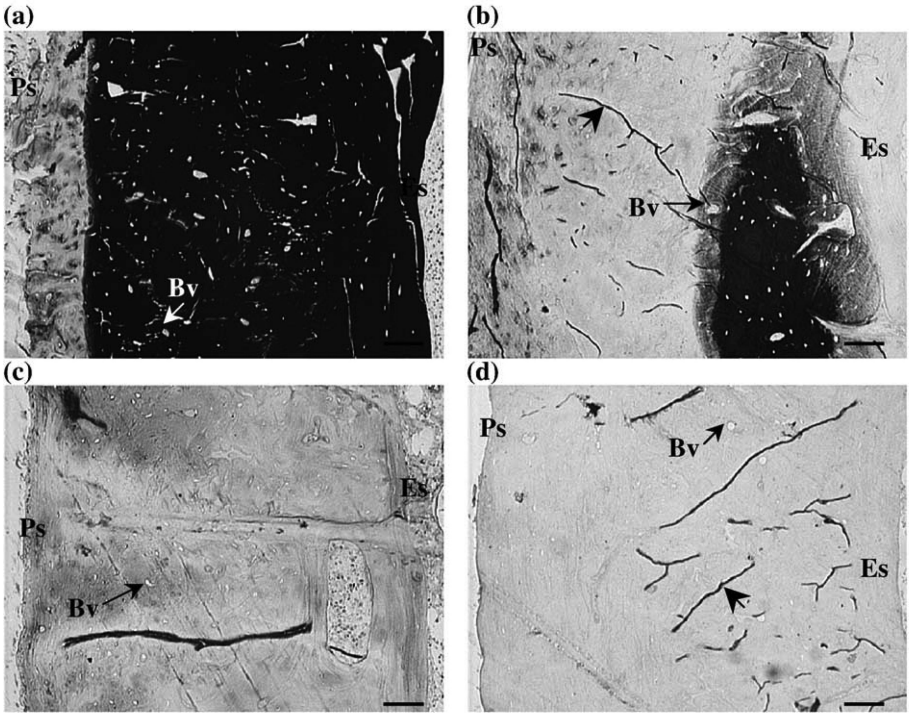

Fig. 5.

Each image shows the femoral mineral content from the periosteal surface (Ps) to the endosteal surface (Es) after the reaction for different times in Perl's reagent: (a) 1 h; (b) 5 h; (c) 8 h; (d) 24 h. The mineral content is qualitatively determined by the brown/black color (in this image by the white/black color) resulting from the reaction of the mineral present in the section and the silver nitrate in the von Kossa solution. (a) After 1 h in Perl's reagent, the section resulted in a partial demineralization toward the periosteal surface (left side of the image), while the rest of the section was still mineralized (black color). (b) 5 h in Perl's reagent almost demineralized the entire section (white part of the image); the only mineral content is indicated by the black color on the right side of the image and by the varying degree of gray/black level just around it. After 8 or 24 h in Perl's reagent (c, d), the samples did not show any mineral content. Blood vessels (Bv) are indicated along with drying artifacts (large arrowheads) caused by the embedding media used (magnification: 8×, scale bar: 50 μm).

Table 1

Different histological processes used

Processing method	Fixative	Perl's reagent	Decalcification	Embedding	Sectioning method
PARA3	2 days in Karnovsky's fixative	3 h	5 days in 10% nitric acid	Paraffin	Microtome
PARA8		8 h	8 days in citrate formic acid		
FROZ1	2 days in Karnovsky's fixative	1 h	24 h in 10% nitric acid	Not embedded; cut with	Cryostat
FROZ3		3h		OCT compound	
FROZ8		8h	None		
FROZ24		24 h			

Key: PARA = paraffin-embedded section; FROZ = frozen, unembedded section.

Table 2

Histomorphometric measurements for the six histological methods (mean ± standard deviation)

	FROZ1	FROZ3	FROZ8	FROZ24	PARA3	PARA8
Total number of blood vessels labeled with ferritin (N.Bv.La)	210 ± 20.4	261 ± 33.6	282 ± 12.6	309 ± 28.0	249 ± 50.3	261 ± 23.2
Total number of blood vessels (N.Bv)	232 ± 12.6	276 ± 33.1	297 ± 9.82	331 ± 26.4	314 ± 36.1	314 ± 29.5
Total number of osteocytes labeled with ferritin (N.Ot.La)	0	0	0	0	0	0
Total number of ferritin halos (N.Ha)	9.00 ± 6.67	9.40 ± 4.39	10.2 ± 9.60	4.20 ± 8.29	17.6 ± 3.58	46.2 ± 5.93

Key: PARA = paraffin-embedded section; FROZ = frozen, unembedded section.